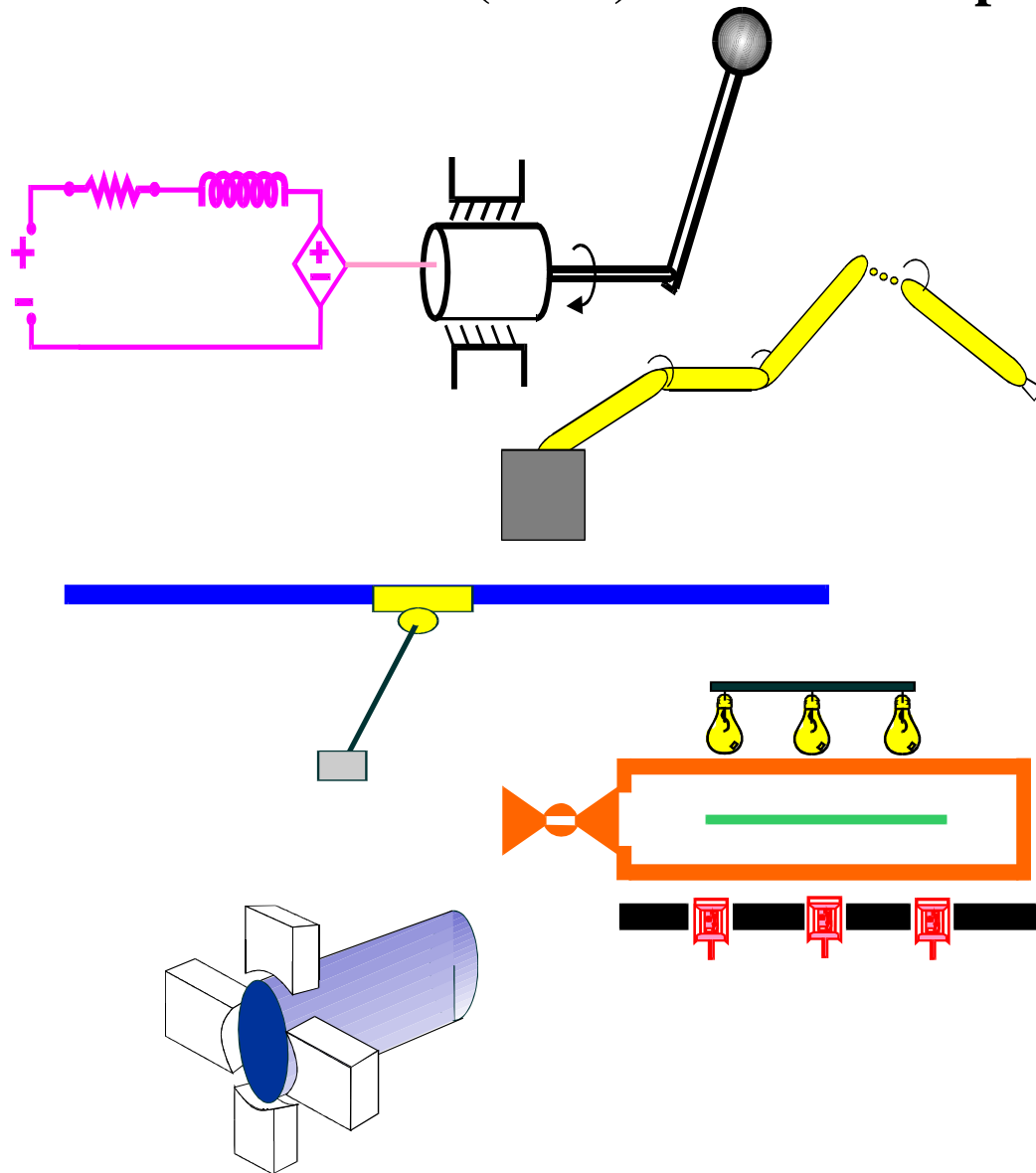


Clemson University
College of Engineering and Science
Control and Robotics (CRB) Technical Report



Number: CU/CRB/2/24/05/#1

Title: Steer-by-Wire Haptic Interface Tracking Controller
Experimental Demonstration

Authors: A. Baviskar, J. Wagner, D. Dawson, and P. Setlur

Steer-by-Wire Haptic Interface Tracking Controller Experimental Demonstration

A. Baviskar, J. Wagner, D. Dawson, and P. Setlur
Automotive Research Laboratory

Departments of Mechanical and Electrical/Computer Engineering
212 Fluor Daniel Engineering Innovation Building, Clemson University
Clemson, South Carolina 29634-0921
voice: (864)656-7376; fax: (864)656-4435; email: jwagner@clemson.edu

1 Introduction

In recent years, engineers and scientists from specialized fields such as information technology, advanced materials, defense systems, and aerospace have collaborated with the automotive industry to introduce advanced technologies for large vehicle production volumes. Examples such as hybrid electric vehicles (HEV) featuring hydrogen, fuel cells, electric motors, solar cells, and/or internal combustion engines are common. Although the concepts of electric and specifically steer-by-wire steering systems have been explored in vehicular research, attention must be focused on the haptic interface. In the robotics field, tele-operation or remote control of robotic manipulators has been well studied and understood as it permits the introduction of human intelligence and decision making capabilities into a possibly hostile remote environment. The concept of force feedback follows directly and its advantage in drive-by-wire vehicles is very evident.

An operator functioning within a remote driving environment primarily depends on visual feedback to make meaningful maneuvers. The “feel” of the road, due to both the vehicle acceleration forces (*i.e.*, G forces) and the tire/road forces, plays a very prominent role in recreating the driving experience [7]. The physiological and psychological effect of these forces has been documented [4]. An appropriate magnitude is important for force feedback to be valuable to the driver. For instance, excessive feedback results in the need for large driver forces to steer the system which defeats the purpose of easing the driving experience. Hence, it is essential for the control strategy to ensure that the road “feel” provided by the force feedback can be adjusted.

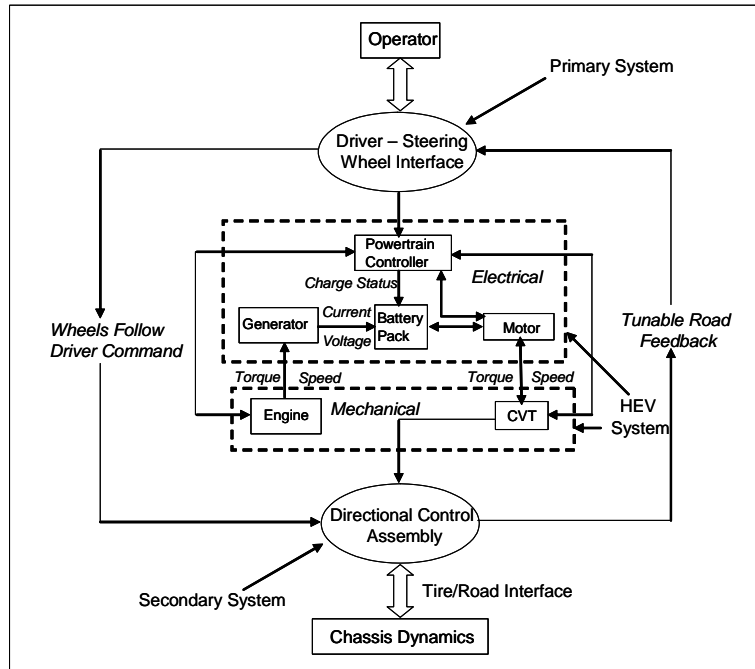


Figure 1: *Steer-by-Wire Interface System Architecture. Signal flow for a typical hybrid vehicle is shown in this figure. It also depicts the idea that input to the Primary System from the operator/driver has to be translated to the Secondary System. At the same time, reaction forces at the Secondary System have to be fed back to the Primary System even though no mechanical linkage exists between these two systems.*

Many researchers have worked on establishing dynamic models and performing experiments to identify system parameters with the intention of providing simulated force feedback ([3], [7], [14]). Detailed modeling of the conventional, electric, and steer-by-wire steering systems is presented in [9]. After making appropriate simplifying assumptions, these models have been utilized in this paper to provide the system model. In [5], the authors design a fuzzy logic controller for active steering system that prevents vehicle spin in wet road conditions. In [6], a novel robot control strategy is designed to force locking between the primary and secondary system while ensuring passivity. Concepts introduced in this paper may be easily extended to add simulated forces on the steering wheel to either ensure safe operation of the vehicle or to communicate the occurrence of certain events (warnings). Theoretical and experimental work ongoing [13] has produced various interesting ideas and results in this area. Present day simulators already use the virtual environment concept to provide safe and realistic learning environment to beginners.

The general concept of the proposed steer-by-wire haptic-interface control architecture is presented in Figure 1. Flow of information in a steering system is bi-

directional. Hence providing force feedback only handles one of the two issues that arise out of decoupling the driver interface and the directional control assembly. The other equally important piece of this system involves the actuation of the directional control assembly to translate the driver’s intentions into actions. In this paper, a full state feedback controller is designed to provide the desired force feedback on the steering wheel to reflect the tire/road interface forces and simultaneously synchronize the motion of the directional control assembly with the motion of the steering wheel. For the force feedback control design, a target system is used to generate the reference signal for the displacement of the primary system. This type of approach is motivated by the impedance control concept detailed in [8]. The controller adapts for parametric uncertainties in the system while ensuring global asymptotic tracking for the “driver experience error” and the “locked error”; however, torque measurements are required.

Finally, to make this concept economically feasible, it is essential to avoid the use of sensors and actuators that are either expensive or require frequent maintenance. Traditionally force/torque sensors have been used to measure the forces that need to be fed back to the driver. However, sensors that can provide the quality of signals necessary for satisfactory performance are both expensive and unreliable. To eliminate torque measurements, a recent idea found in [12] has been modified to develop torque observers for the design of an exact model knowledge tracking controller. This controller ensures that the torque observation error converges asymptotically to zero while also ensuring global asymptotic tracking for the driver experience error and the locked tracking error. Roughly speaking, the torque observer design borrows concepts from robust control techniques that only impose boundedness and smoothness restrictions on the unmeasurable torque signals.

This article is organized as follows. In Section 2, the control system objectives are stated. In Section 3, the models for the servo-motor based steering system and the target signal generator are presented followed by the open-loop tracking dynamics. In Section 4, an adaptive, tracking controller is presented along with the corresponding closed-loop error system. The stability analysis is discussed in Section 5. In Section 6, the controller is redesigned to obtain an exact model knowledge tracking controller, the eliminates torque measurements, followed by representative numerical simulation results in Section 7. The description of the test bench along with the experimental verification of the controllers are presented in Section 8. Concluding remarks are presented in Section 9.

2 Control Problem Statement

The steer-by-wire haptic interface control objective is twofold. First, the driver’s steering angle commands must be accurately followed; this requires the torque control input provided by the drive motor to be designed so that the angular position of the directional control assembly accurately tracks the input. Second, the driver must

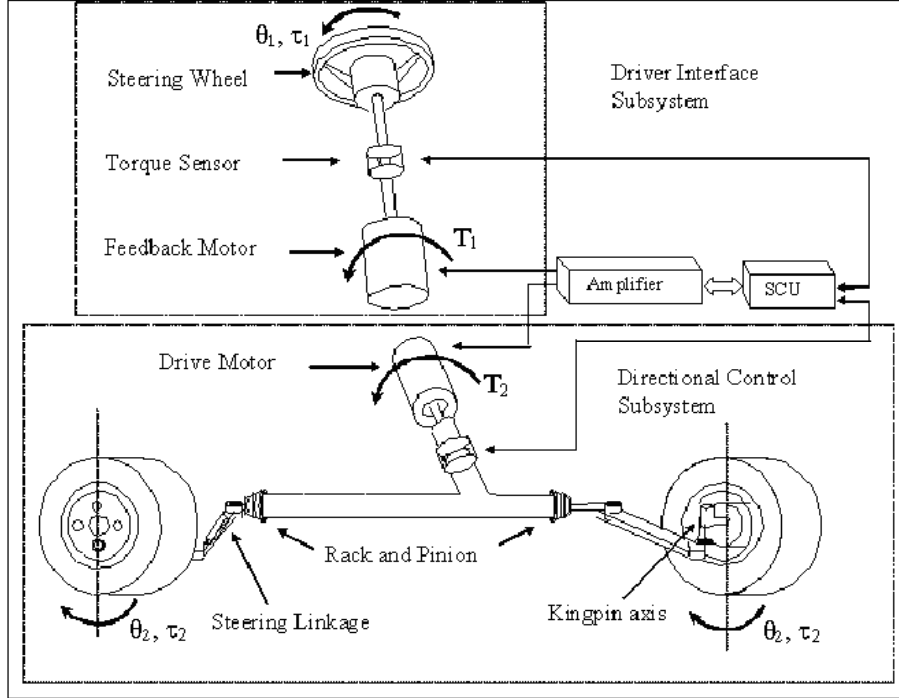


Figure 2: *Driver interface and directional control subsystems in a steer-by-wire assembly with nomenclature. The figure depicts the essential components present in a steer-by-wire system. The nomenclature gives an idea about the various signals considered in the paper.*

be given a realistic “virtual driving experience”. To this end, a reference model, or target dynamics for the driver input device, should be designed to generate the desired angular position of the driver input device. The control torque provided by the feedback motor must then be designed to ensure that the response of the driver input device follows that of the reference system. The reader is referred to Figure 2 for definition of the driver interface and the directional control assembly.

3 Dynamic Model Development

Detailed models for the conventional and power assisted steering systems can be found in many works in this research area (*e.g.*, [9], [10]). The steer-by-wire system involves the removal of the steering column present in a conventional steering system and the introduction of two servo motors. The steering system is separated into two subsystems: the primary and the secondary subsystems. The primary system, consists of the driver input device (*e.g.*, steering wheel or joystick) and a servo motor to provide the driver with force feedback. The secondary subsystem, is composed

of the directional control assembly (*e.g.*, rack and pinion system) and a servo motor that provides the necessary torque input to drive this assembly and steer the vehicle.

3.1 Steering System Model Formulation

In general, the steering system dynamics, may be expressed in a simplified form as

$$I_1 \ddot{\theta}_1 + N_1(\theta_1, \dot{\theta}_1) = \alpha_1 \tau_1 + T_1 \quad (1)$$

$$I_2 \ddot{\theta}_2 + N_2(\theta_2, \dot{\theta}_2) = \alpha_2 \tau_2 + T_2 \quad (2)$$

where $\theta_1(t)$, $\dot{\theta}_1(t)$, $\ddot{\theta}_1(t) \in \mathfrak{R}^1$ denote the angular position, velocity, and acceleration, respectively, of the driver input device, $I_1, I_2 \in \mathfrak{R}^1$ represent the inertias of the driver input device and the vehicle directional control assembly, respectively. $N_1(\theta_1, \dot{\theta}_1) \in \mathfrak{R}^1$ is an auxiliary nonlinear function that describes the dynamics on the driver side, $\tau_1(t) \in \mathfrak{R}^1$ denotes the driver input torque, $T_1(t) \in \mathfrak{R}^1$ represents a control input torque applied to the driver input device, $\theta_2(t)$, $\dot{\theta}_2(t)$, $\ddot{\theta}_2(t) \in \mathfrak{R}^1$ denote the angular position, velocity, and acceleration, respectively, of the vehicle directional control assembly, $N_2(\theta_2, \dot{\theta}_2) \in \mathfrak{R}^1$ is an auxiliary nonlinear function that is used to describe the dynamics of the vehicle directional control assembly, $\tau_2(t) \in \mathfrak{R}^1$ represents the reaction torque between the actuator on the directional control assembly and mechanical subsystem actuated by the directional control assembly, and $T_2(t) \in \mathfrak{R}^1$ denotes a control input torque applied to the directional control assembly. The constants $\alpha_1, \alpha_2 \in \mathfrak{R}^1$ are scaling factors that could arise due to gearing in the system.

Remark 1 *The damping and friction effects modeled by $N_1(\cdot)$ and $N_2(\cdot)$ are assumed to be linearly parameterizable as*

$$N_1(\theta_1, \dot{\theta}_1) = Y_{N1}(\theta_1, \dot{\theta}_1) \phi_{N1} \quad (3)$$

$$N_2(\theta_2, \dot{\theta}_2) = Y_{N2}(\theta_2, \dot{\theta}_2) \phi_{N2}. \quad (4)$$

where $Y_{N1}(\cdot) \in \mathfrak{R}^{1 \times p}$, $Y_{N2}(\cdot) \in \mathfrak{R}^{1 \times q}$ are regression matrices containing the measurable signals, and $\phi_{N1} \in \mathfrak{R}^{p \times 1}$, $\phi_{N2} \in \mathfrak{R}^{q \times 1}$ are constant matrices containing the unknown parameters in the model $N_1(\cdot)$ and $N_2(\cdot)$. Further, it is also assumed that if $\theta_1(t), \dot{\theta}_1(t) \in \mathcal{L}_\infty$ then $N_1(\theta_1, \dot{\theta}_1) \in \mathcal{L}_\infty$ and if $\theta_2(t), \dot{\theta}_2(t) \in \mathcal{L}_\infty$ then $N_2(\theta_2, \dot{\theta}_2) \in \mathcal{L}_\infty$.

3.2 Reference Model Development

The second control objective is the provision of road “feel” to the driver. To satisfy this goal, impedance control concepts [8] used for robot manipulator position/force

control problems have been applied to the problem. Specifically, a reference model is designed as

$$I_T \ddot{\theta}_{d1} + N_T(\theta_{d1}, \dot{\theta}_{d1}) = \alpha_{T1}\tau_1 + \alpha_{T2}\tau_2 \quad (5)$$

where $\theta_{d1}(t)$, $\dot{\theta}_{d1}(t)$, $\ddot{\theta}_{d1}(t) \in \mathfrak{R}^1$ denote the desired angular position, velocity, and acceleration, respectively, of the driver input device, $N_T(\theta_{d1}, \dot{\theta}_{d1}) \in \mathfrak{R}^1$ represents an auxiliary target dynamic function for the driver input device, and $\alpha_{T1}, \alpha_{T2} \in \mathfrak{R}^1$ are scaling constants. The structure for (5) is motivated by the following philosophy: If $T_1(t)$ was exactly equal to $\alpha_2\tau_2(t)$ in (1), then the dynamics given by (1) would give the driver a realistic experience provided the auxiliary term $N_1(\cdot)$ in (1) could be designed or constructed according to some desirable mechanical response. Thus, the $N_T(\cdot)$ term in (5) is designed to simulate the desired driving experience, and hence, the dynamics given by (5) serve as a desired trajectory generator for control design purposes for (1).

Remark 2 *The target dynamic function $N_T(\cdot)$ must be selected to ensure that the desired driver input device trajectory and its first two derivatives remain bounded at all time (i.e., $\theta_{d1}(t), \dot{\theta}_{d1}(t), \ddot{\theta}_{d1}(t) \in \mathcal{L}_\infty$). Suppose $N_T(\cdot)$ is selected as*

$$N_T = B_T \dot{\theta}_{d1} + K_T \theta_{d1} \quad (6)$$

where $B_T, K_T \in \mathfrak{R}^1$ are some positive design constants. If $N_T(\cdot)$ is selected according to (6), then standard linear arguments show that $\theta_{d1}(t), \dot{\theta}_{d1}(t), \ddot{\theta}_{d1}(t) \in \mathcal{L}_\infty$. Furthermore, $N_T(\cdot)$ can be constructed as a nonlinear “damping” function by utilizing Lyapunov type arguments.

3.3 Open-Loop Error System Development

To quantify the mismatches between the target system and the primary system or driver experience tracking error, as well as the primary and the secondary system or locked tracking error, filtered error signals, $r_1(t), r_2(t) \in \mathfrak{R}^1$ are defined as

$$r_1 = \dot{e}_1 + \mu_1 e_1 \quad (7)$$

$$r_2 = \dot{e}_2 + \mu_2 e_2 \quad (8)$$

where $\mu_1, \mu_2 \in \mathfrak{R}^1$ represent positive control gains, and the error signals $e_1(t), e_2(t) \in \mathfrak{R}^1$ are

$$e_1 = \theta_{d1} - \theta_1 \quad (9)$$

$$e_2 = \theta_1 - \theta_2. \quad (10)$$

After taking the first time derivative of (7) and (8), and substituting the dynamics in (1), (2) and (5), the open loop error systems are

$$I_1 \dot{r}_1 = Y_1 \phi_1 - T_1 \quad (11)$$

$$I_2 \dot{r}_2 = Y_2 \phi_2 - T_2 \quad (12)$$

where $Y_1(\cdot) \in \mathfrak{R}^{1 \times r}$, $Y_2(\cdot) \in \mathfrak{R}^{1 \times s}$ are regression matrices consisting of measurable quantities, and $\phi_1 \in \mathfrak{R}^{r \times 1}$, $\phi_2 \in \mathfrak{R}^{s \times 1}$ are constant unknown vectors. The reader is referred to Appendix A for explicit definitions of $Y_1(\cdot)$, $Y_2(\cdot)$, ϕ_1 and ϕ_2 .

Remark 3 *Based on the definition of $r_1(t)$ and $r_2(t)$ given in (7) and (8), standard arguments [1] can be used to prove that: (i) if $r_1(t)$, $r_2(t) \in \mathcal{L}_\infty$, then $e_1(t)$, $e_2(t)$, $\dot{e}_1(t)$, $\dot{e}_2(t) \in \mathcal{L}_\infty$, and (ii) if $r_1(t)$ and $r_2(t)$ are asymptotically regulated, then $e_1(t)$ and $e_2(t)$ are asymptotically regulated.*

4 Control Development

The first control objective requires the target following and the locked tracking error signals to approach zero asymptotically, while adapting for the system parameters that are assumed to be unknown. Further, the signals $\theta_1(t)$, $\theta_2(t)$, $\dot{\theta}_1(t)$, $\dot{\theta}_2(t)$, $\tau_1(t)$, and $\tau_2(t) \in \mathcal{L}_\infty$ must be available for measurement.

4.1 Control Formulation

Based on the subsequent stability analysis in Section 5 and the structure of the open-loop error system given in (11) and (12), the control inputs $T_1(t)$ and $T_2(t)$ are designed as

$$T_1 = k_1 r_1 + Y_1 \hat{\phi}_1 \quad (13)$$

$$T_2 = k_2 r_2 + Y_2 \hat{\phi}_2 \quad (14)$$

where $k_1, k_2 \in \mathfrak{R}^1$ are constant positive control gains, and $\hat{\phi}_1(t) \in \mathfrak{R}^{r \times 1}$, $\hat{\phi}_2(t) \in \mathfrak{R}^{s \times 1}$ are adaptive estimates for the unknown parameter matrices. The adaptive update laws are designed based on the subsequent stability analysis as

$$\dot{\hat{\phi}}_1 = \Gamma_1 Y_1^T r_1 \quad (15)$$

$$\dot{\hat{\phi}}_2 = \Gamma_2 Y_2^T r_2 \quad (16)$$

where $\Gamma_1 \in \mathfrak{R}^{r \times r}$, $\Gamma_2 \in \mathfrak{R}^{s \times s}$ are positive constant diagonal gain matrices.

4.2 Closed-Loop Error System Development

After substituting the control torques in (13) and (14) into the open-loop dynamics in (11) and (12), the closed-loop error system becomes

$$I_1 \dot{r}_1 = -k_1 r_1 + Y_1 \tilde{\phi}_1 \quad (17)$$

$$I_2 \dot{r}_2 = -k_2 r_2 + Y_2 \tilde{\phi}_2 \quad (18)$$

where the parameter estimation error signals, $\tilde{\phi}_1(t) \in \mathfrak{R}^{r \times 1}$, $\tilde{\phi}_2(t) \in \mathfrak{R}^{s \times 1}$ are defined as

$$\tilde{\phi}_1 = \phi_1 - \hat{\phi}_1 \quad (19)$$

$$\tilde{\phi}_2 = \phi_2 - \hat{\phi}_2. \quad (20)$$

5 Stability Analysis

Theorem 1 *Given the closed-loop system of (17) and (18), the tracking error signals defined in (9) and (10) are globally asymptotically regulated in the sense that*

$$\lim_{t \rightarrow \infty} e_1(t), e_2(t) = 0. \quad (21)$$

Proof: A non-negative, scalar function, denoted by $V(t) \in \mathfrak{R}^1$, is defined as

$$V = \frac{1}{2} I_1 r_1^2 + \frac{1}{2} I_2 r_2^2 + \frac{1}{2} \tilde{\phi}_1^T \Gamma_1^{-1} \tilde{\phi}_1 + \frac{1}{2} \tilde{\phi}_2^T \Gamma_2^{-1} \tilde{\phi}_2. \quad (22)$$

After taking the time derivative of (22) and making the appropriate substitutions from (17), (18), (19), and (20), the following expression is obtained

$$\begin{aligned} \dot{V} = & r_1 \left[-k_1 r_1 + Y_1 \tilde{\phi}_1 \right] + r_2 \left[-k_2 r_2 + Y_2 \tilde{\phi}_2 \right] \\ & - \tilde{\phi}_1^T \left[Y_1^T r_1 \right] - \tilde{\phi}_2^T \left[Y_2^T r_2 \right] \end{aligned} \quad (23)$$

where the fact that Γ_1, Γ_2 are constant diagonal gain matrices has been utilized along with the following equalities $\dot{\tilde{\phi}}_1 = -\dot{\hat{\phi}}_1$ and $\dot{\tilde{\phi}}_2 = -\dot{\hat{\phi}}_2$.

After cancelling common terms, it is easy to see that we can upper bound $\dot{V}(t)$ as follows

$$\dot{V} \leq -k_1 r_1^2 - k_2 r_2^2. \quad (24)$$

From (24) and (22), it is straightforward to see that $r_1(t), r_2(t), \tilde{\phi}_1(t), \tilde{\phi}_2(t) \in \mathcal{L}_\infty$. After utilizing (19), (20), and Remark 3, we can conclude that $e_1(t), \dot{e}_1(t), e_2(t), \dot{e}_2(t), \hat{\phi}_1(t), \hat{\phi}_2(t) \in \mathcal{L}_\infty$. Using Remark 2, (9), (10) and their first derivatives, it is clear that $\theta_1(t), \theta_2(t), \dot{\theta}_1(t), \dot{\theta}_2(t) \in \mathcal{L}_\infty$. From the explicit definition for $Y_1(\cdot)$ given in Appendix A and using the fact that $\tau_1(t), \tau_2(t) \in \mathcal{L}_\infty$, it is easy to see that $Y_1(\cdot) \in \mathcal{L}_\infty$. From (13), it is clear that the control torque $T_1(t) \in \mathcal{L}_\infty$. Again, from the definition of $Y_2(\cdot)$ in Appendix A and from the above facts, $Y_2(\cdot) \in \mathcal{L}_\infty$. From (14), it is clear that $T_2(t) \in \mathcal{L}_\infty$. Using standard signal chasing arguments, it can be shown that all the signals in the closed-loop system remain bounded. In particular, from (17) and (18), $\dot{r}_1(t), \dot{r}_2(t) \in \mathcal{L}_\infty$. After employing a corollary to Barbalat's Lemma [16], it is easy to show that

$$\lim_{t \rightarrow \infty} r_1(t), r_2(t) = 0.$$

Finally, Remark 3 can be used to prove the result stated in (21).

6 Elimination of Torque Measurements: Extension

For the steering system in (1) and (2), a controller can be designed to eliminate the need for torque sensors. Here the assumption is that the driver input torque, denoted by $\tau_1(t)$, and the reaction torque between the actuator on the directional control assembly and mechanical subsystem actuated by the directional control assembly, denoted by $\tau_2(t)$, are not available for measurement. Another assumption is that the dynamics are exactly known with the exception of the torque signals $\tau_1(t)$ and $\tau_2(t)$, and that the signals $\theta_1(t)$, $\theta_2(t)$, $\dot{\theta}_1(t)$, and $\dot{\theta}_2(t)$ are available for measurement. To account for the lack of torque measurements, the torque observation errors, denoted by $\tilde{\tau}_1(t)$, $\tilde{\tau}_2(t) \in \mathfrak{R}^1$, are defined as

$$\tilde{\tau}_1 = \tau_1 - \hat{\tau}_1 \quad (25)$$

$$\tilde{\tau}_2 = \tau_2 - \hat{\tau}_2 \quad (26)$$

where $\hat{\tau}_1(t)$, $\hat{\tau}_2(t) \in \mathfrak{R}^1$ denote the driver input and the reaction observer torques, respectively. The observer torques are subsequently designed in Section 6.2. The target dynamics are now generated as

$$I_T \ddot{\theta}_{d1} + N_T(\theta_{d1}, \dot{\theta}_{d1}) = \alpha_{T1} \hat{\tau}_1 + \alpha_{T2} \hat{\tau}_2. \quad (27)$$

Remark 4 *It is assumed that the driver input torque $\tau_1(t)$ and the reaction torque $\tau_2(t)$ and their first two derivatives remain bounded at all times which means $\tau_1(t)$, $\dot{\tau}_1(t)$, $\ddot{\tau}_1(t)$, $\tau_2(t)$, $\dot{\tau}_2(t)$, $\ddot{\tau}_2(t) \in \mathcal{L}_\infty$.*

6.1 Open-Loop Error System Development

After taking two time derivatives of (9) and (10), and substituting the dynamics given in (1) and (2) and the target dynamics given in (27), the open loop error systems for the two systems can be written as

$$\ddot{e}_1 = \left(\frac{1}{I_T}\right) (-N_T(\cdot) + \alpha_{T1} \hat{\tau}_1 + \alpha_{T2} \hat{\tau}_2) - \left(\frac{1}{I_1}\right) (-N_1(\cdot) + \alpha_1 \tau_1 + T_1) \quad (28)$$

$$\ddot{e}_2 = \left(\frac{1}{I_1}\right) (-N_1(\cdot) + \alpha_1 \tau_1 + T_1) - \left(\frac{1}{I_2}\right) (-N_2(\cdot) + \alpha_2 \tau_2 + T_2). \quad (29)$$

To simplify further analysis, two filtered tracking error signals, denoted by $s_1(t)$, $s_2(t) \in \mathfrak{R}^1$, are

$$s_1 = \ddot{e}_1 + (\beta_1 + 1) \dot{e}_1 + \beta_1 e_1 \quad (30)$$

$$s_2 = \ddot{e}_2 + (\beta_1 + 1) \dot{e}_2 + \beta_1 e_2 \quad (31)$$

where $\beta_1 \in \mathfrak{R}^1$ is a constant positive control gain.

6.2 Control Development

Based on the subsequent stability analysis, subsequent control design, and the structure of the open-loop error system given by (28) and (29), the driver input torque observer and the reaction torque observer are

$$\dot{\hat{\tau}}_1 = -(\beta_1 + K_s + 1)\hat{\tau}_1 - \frac{I_1}{\alpha_1} [(\beta_1 + K_s(\beta_1 + 1))\dot{e}_1 + K_s\beta_1 e_1 + \rho_1 \text{sgn}(p_1)] \quad (32)$$

$$\begin{aligned} \dot{\hat{\tau}}_2 = & -(\beta_1 + K_s + 1)\hat{\tau}_2 - \frac{I_2}{\alpha_2} [(\beta_1 + K_s(\beta_1 + 1))\dot{e}_2 + K_s\beta_1 e_2] \\ & - \frac{I_2}{\alpha_2} \left[\frac{\alpha_1}{I_1} \left(\dot{\hat{\tau}}_1 + (\beta_1 + K_s + 1)\hat{\tau}_1 \right) + \rho_2 \text{sgn}(p_2) \right] \end{aligned} \quad (33)$$

where $\text{sgn}(\cdot)$ denotes the standard signum function, $K_s, \rho_1, \rho_2 \in \mathfrak{R}^1$ are positive control gains and the auxiliary signals $p_1(t), p_2(t) \in \mathfrak{R}^1$ are defined as

$$p_1 = \dot{e}_1 + \beta_1 e_1 \quad (34)$$

$$p_2 = \dot{e}_2 + \beta_1 e_2 \quad (35)$$

where β_1 was introduced in (30) and (31). Based on the subsequent stability analysis, the control inputs $T_1(t)$ and $T_2(t)$ are designed as

$$T_1 = N_1(\cdot) + \left(\frac{I_1}{I_T} \right) (-N_T(\cdot) + \alpha_{T1}\hat{\tau}_1 + \alpha_{T2}\hat{\tau}_2) - \alpha_1\hat{\tau}_1 \quad (36)$$

$$T_2 = N_2(\cdot) + \left(\frac{I_2}{I_1} \right) (-N_1(\cdot) + T_1 + \alpha_1\hat{\tau}_1) - \alpha_2\hat{\tau}_2. \quad (37)$$

Remark 5 *To facilitate the subsequent stability analysis, two auxiliary “disturbance signals”, denoted by $\eta_1(t), \eta_2(t) \in \mathfrak{R}^1$, are defined as*

$$\eta_1 = \left(\frac{\alpha_1}{I_1} \right) (\dot{\hat{\tau}}_1 + (\beta_1 + K_s + 1)\hat{\tau}_1) \quad (38)$$

$$\eta_2 = \left(\frac{\alpha_2}{I_2} \right) (\dot{\hat{\tau}}_2 + (\beta_2 + K_{s2} + 1)\hat{\tau}_2). \quad (39)$$

Based on Remark 4, $\eta_1(t), \eta_2(t), \dot{\eta}_1(t), \dot{\eta}_2(t) \in \mathcal{L}_\infty$. The definitions of (38) and (39), permit the subsequent closed-loop error system development and the stability analysis are facilitated by selecting the control gains ρ_1 and ρ_2 , introduced in (32) and (33), as

$$\rho_1 \geq |\eta_1| + \left| \frac{d\eta_1(\sigma)}{d\sigma} \right| \quad (40)$$

$$\rho_2 \geq |\eta_2| + \left| \frac{d\eta_2(\sigma)}{d\sigma} \right| + \rho_1. \quad (41)$$

6.3 Closed-Loop Error System Development

The control torques in (36) and (37) maybe substituted into the open-loop dynamics in (28) and (28), so that the closed-loop error system becomes

$$\ddot{e}_1 = -\left(\frac{\alpha_1}{I_1}\right)(\tau_1 - \hat{\tau}_1) \quad (42)$$

$$\ddot{e}_2 = \left(\frac{\alpha_1}{I_1}\right)(\tau_1 - \hat{\tau}_1) - \left(\frac{\alpha_2}{I_2}\right)(\tau_2 - \hat{\tau}_2). \quad (43)$$

After taking the first time derivative of (30) and (31), and using (42), (43), and their first derivatives, the closed-loop error system becomes

$$\dot{s}_1 = -K_s s_1 - \eta_1 - \rho_1 \text{sgn}(p_1) \quad (44)$$

$$\dot{s}_2 = -K_s s_2 + \eta_1 - \eta_2 - \rho_2 \text{sgn}(p_2) \quad (45)$$

where (38), (39), (32), and (33) have been utilized.

Remark 6 *Based on the definition of $s_1(t)$ and $s_2(t)$ given in (30) and (31), extensions of the arguments made in [1] can be used to prove that: (i) if $s_1(t), s_2(t) \in \mathcal{L}_\infty$, then $e_1(t), e_2(t), \dot{e}_1(t), \dot{e}_2(t), \ddot{e}_1(t), \ddot{e}_2(t) \in \mathcal{L}_\infty$, and (ii) if $s_1(t)$ and $s_2(t)$ are asymptotically regulated, then $e_1(t), e_2(t), \dot{e}_1(t), \dot{e}_2(t), \ddot{e}_1(t), \ddot{e}_2(t)$ are also asymptotically regulated [2].*

6.4 Stability Proof

Theorem 2 *Given the closed-loop system of (44) and (45), the tracking error signals defined in (9) and (10) along with the torque observation errors defined in (25) and (26) are globally asymptotically regulated in the sense that*

$$\lim_{t \rightarrow \infty} e_1(t), e_2(t), \tilde{\tau}_1(t), \tilde{\tau}_2(t) = 0. \quad (46)$$

Proof: A non-negative, scalar function, denoted by $V_{a1}(t) \in \mathfrak{R}^1$, is defined as

$$V_{a1} = \frac{1}{2}s_1^2. \quad (47)$$

After taking the time derivative of (47) and making appropriate substitutions from (44), then $\dot{V}_{a1}(t)$ maybe expressed as

$$\dot{V}_{a1} = -K_s s_1^2 + (\dot{p}_1 + p_1)(-\eta_1 - \rho_1 \text{sgn}(p_1)) \quad (48)$$

where the definitions of $s_1(t)$ and $p_1(t)$ given in (30) and (34) have been utilized. After integrating both sides of (48), and performing some mathematical operations

(refer to Appendix B), the following inequality can be obtained

$$\begin{aligned}
V_{a1}(t) - V_{a1}(t_0) \leq & -K_s \int_{t_0}^t s_1^2(\sigma) d\sigma \\
& + \left[\int_{t_0}^t |p_1(\sigma)| \left(|\eta_1| + \left| \frac{d\eta_1(\sigma)}{d\sigma} \right| - \rho_1 \right) d\sigma \right] \\
& + [|p_1| (|\eta_1| - \rho_1)] + \eta_1(t_0) p_1(t_0) + \rho_1 |p_1(t_0)|
\end{aligned} \tag{49}$$

After applying (40) to the bracketed terms in (49), $V_{a1}(t)$ can be upper bounded as

$$V_{a1}(t) \leq V_{a1}(t_0) - K_s \int_{t_0}^t s_1^2(\sigma) d\sigma + \zeta_{01} \tag{50}$$

where $\zeta_{01} \in \mathfrak{R}^1$ is a positive constant defined as

$$\zeta_{01} = \eta_1(t_0) p_1(t_0) + \rho_1 |p_1(t_0)|. \tag{51}$$

For the error system given in (45), a second non-negative, scalar function, denoted by $V_{a2}(t) \in \mathfrak{R}^1$, is

$$V_{a2} = \frac{1}{2} s_2^2. \tag{52}$$

Following a similar analysis to that presented above, the upper bound for $V_{a2}(t)$ becomes

$$V_{a2}(t) \leq V_{a2}(t_0) - K_s \int_{t_0}^t s_2^2(\sigma) d\sigma + \zeta_{02} \tag{53}$$

where $\zeta_{02} \in \mathfrak{R}^1$ is a positive constant defined as

$$\zeta_{02} = \eta_2(t_0) p_2(t_0) - \eta_1(t_0) p_2(t_0) + \rho_2 |p_2(t_0)|. \tag{54}$$

To complete the analysis, the following composite non-negative, scalar function, $V_a(t) \in \mathfrak{R}^1$, is selected

$$V_a = V_{a1} + V_{a2} = \frac{1}{2} s_1^2 + \frac{1}{2} s_2^2. \tag{55}$$

After using the bounds for $V_{a1}(t)$ and $V_{a2}(t)$ obtained in (50) and (53), the upper bound for $V_a(t)$ becomes

$$V_a(t) \leq V_a(t_0) - K_s \int_{t_0}^t s_1^2(\sigma) d\sigma - K_s \int_{t_0}^t s_2^2(\sigma) d\sigma + \zeta_0 \tag{56}$$

where $\zeta_0 = \zeta_{01} + \zeta_{02}$. Clearly, from the inequality in (56), $V_a(t) \in \mathcal{L}_\infty$. From the definition of $V_a(t)$ in (55), $s_1(t), s_2(t) \in \mathcal{L}_\infty$. From Remark 6, $e_1(t), e_2(t), \dot{e}_1(t)$,

$\dot{e}_2(t)$, $\ddot{e}_1(t)$, $\ddot{e}_2(t) \in \mathcal{L}_\infty$. From (44), (45), (34) and (35) and Remark 5, it is easy to see that $\dot{s}_1(t)$, $\dot{s}_2(t)$, $p_1(t)$, $p_2(t) \in \mathcal{L}_\infty$. From (42) and (43), it is now clear that $\hat{\tau}_1(t)$, $\hat{\tau}_2(t) \in \mathcal{L}_\infty$. From equation (36), it can be shown that $T_1(t) \in \mathcal{L}_\infty$. Using this fact, it is easy to see from (37) that $T_2(t) \in \mathcal{L}_\infty$. Standard signal chasing arguments can now be employed to show that all signals in the system remain bounded. If (56) is rewritten as

$$K_s \int_{t_0}^t s_1^2(\sigma) d\sigma + K_s \int_{t_0}^t s_2^2(\sigma) d\sigma \leq V_a(t) - V_a(t_0) + \zeta_0, \quad (57)$$

then it is clear that $s_1(t)$, $s_2(t) \in \mathcal{L}_2$. Further, Barbalat's Lemma [16] can be applied to show that

$$\lim_{t \rightarrow \infty} s_1(t), s_2(t) = 0, \quad (58)$$

and hence, from Remark 6,

$$\lim_{t \rightarrow \infty} e_1(t), e_2(t), \dot{e}_1(t), \dot{e}_2(t), \ddot{e}_1(t), \ddot{e}_2(t) = 0. \quad (59)$$

Since $\ddot{e}_1(t)$ and $\ddot{e}_2(t)$ are regulated to zero as indicated by (59), then (42) and (43) and the definitions provided in (25) and (26) show that

$$\lim_{t \rightarrow \infty} \tilde{\tau}_1(t), \tilde{\tau}_2(t) = 0. \quad (60)$$

Remark 7 *The structure of the torque observers given by (32) and (33) contain discontinuous terms; however, the control inputs that are applied to the plant are not discontinuous. That is, after a close examination of (32) and (33), it is clear that signals $\hat{\tau}_1(t)$ and $\hat{\tau}_2(t)$ are low pass filtered outputs of a discontinuous control signal. Therefore, the control strategy only utilizes the signals $\hat{\tau}_1(t)$ and $\hat{\tau}_2(t)$, so that the control signals applied to the plant will not be discontinuous.*

7 Numerical Simulation Results

Two sets of simulations were performed to study the performance of the control algorithms: (i) System with an adaptive controller as developed in Section 4, and (ii) System with a exact model knowledge controller (EMK controller) presented in Section 6. The simulated vehicle steering system was assumed to have the dynamics described by (1) and (2). The nonlinear damping and friction functions were chosen [9] as

$$N_i(\theta_i, \dot{\theta}_i) = B_i \dot{\theta}_i + K_i \theta_i \quad i = 1, 2 \quad (61)$$

The system parameters were chosen to be the same as that of the actual experimental setup described in Section 8. These values are listed in Table 1.

Variable	Value	Units	Variable	Value	Units
I_1	1.16×10^{-2}	$kg - m^2$	I_T	1.5×10^{-2}	$kg - m^2$
B_1	1.9×10^{-2}	$kg - m^2/s$	B_T	2×10^{-2}	$kg - m^2/s$
K_1	0	$N - m$	K_T	0	$N - m$
α_1	1	—	α_{T1}	1	—
I_2	2.35×10^{-2}	$kg - m^2$	α_{T2}	0.15	—
B_2	0.6	$kg - m^2/s$	C_d	150	$N - m$
K_2	0	$N - m$	γ	0.02	—
α_2	1	—			

Table 1: List of Simulation Parameters and Corresponding Values

The reference trajectory was generated according to (5). The user defined function $N_T(\theta_{d1}, \dot{\theta}_{d1})$ was chosen to have the same form as in (61). The reaction torque applied on the directional control assembly (due to the tire-road interface forces), was assumed to be related to the angular deflection of the directional control assembly in the following manner [15]

$$\tau_2 = -C_d \tanh(\gamma\theta_2) \quad (62)$$

where $C_d, \gamma \in \mathfrak{R}^1$ are constant tire-dependent parameters listed in Table 1. Each set of simulations were performed for two driver input torque profiles: *Case 1*: $\tau_1(t) = 0.8 \sin(5t)(1 - \exp(-3t))$ which represents the input to perform a standard slalom maneuver; and *Case 2*: $\tau_1(t) = 0.9(1 - \exp(-3t))$ which is the input that the driver would apply to follow a circular trajectory (refer to Figure 3).

For the first set of simulations, the torque “measurements” are directly available for use in the control algorithm as opposed to torque observer estimation. All adaptive estimates were initialized to zero in this simulation. The driver experience and locked tracking errors, $e_1(t)$ and $e_2(t)$, are presented in Figure (4). The driver experience tracking error corresponds to the differences between the target and the primary subsystem of the haptic interface steer-by-wire system. As shown, the error $e_1(t)$ approaches zero after $t = 5s$ for both inputs which implies that the driver experiences the desired “feel” as specified by the target parameters (which corresponds to a conventional steering system with the target parameters). The locked tracking error, $e_2(t)$, also approaches zero for both inputs. This demonstrates that the driver’s steering commands are followed by the directional control assembly. These two facts prove that the control algorithm achieves the two goals outlined in the control objective (refer to Section 2 for details). All the parameter estimates were observed to settle down at constant values. The plots for adaptive estimates have been left out for brevity. The corresponding motor control torques are displayed in Figure 5. Due to the significantly higher dynamic friction parameter, B_2 , of the secondary subsys-

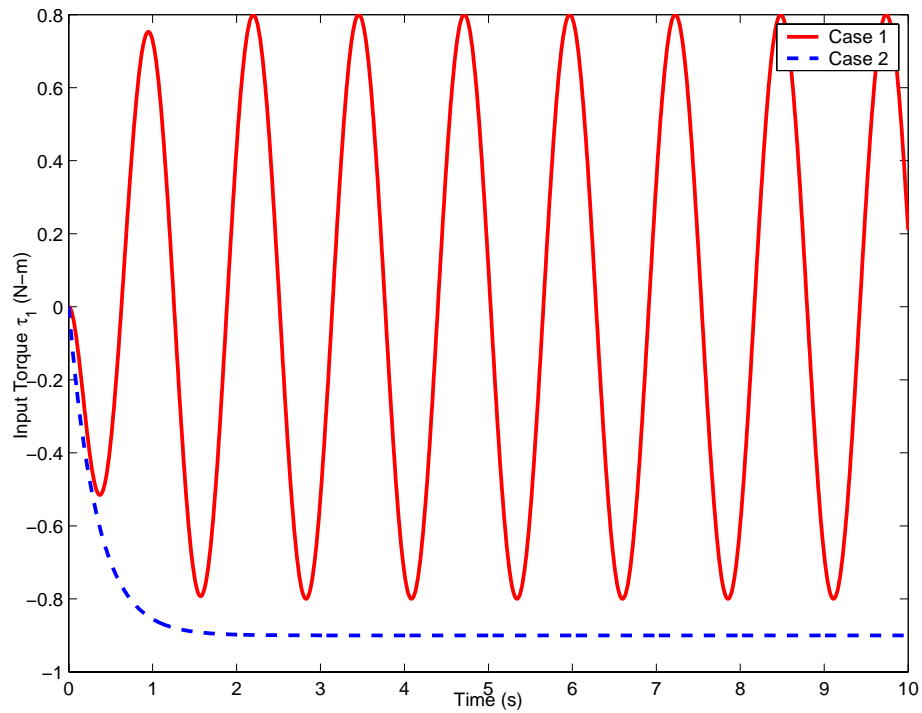


Figure 3: Driver input torque profiles for steering, $\tau_1(t)$. Case 1 is a representation of driver's steering input to perform slalom maneuver and Case 2 represents the driver's steering input for the vehicle to follow a circular trajectory.

Performance Measure	Case 1		Case 2	
	e_1	e_2	e_1	e_2
Peak Error (%)	0.0577	0.9755	0.9351	2.4913
Steady-State Error (%)	0	0.001	0.0002	0.0025
Settling time (s)	—	—	2.297	2.285

Table 2: Summary of Results for Adaptive Controller Simulation

Performance Measure	Case 1		Case 2	
	e_1	e_2	e_1	e_2
Peak Error (%)	0.0222	0.0644	0.1521	0.0698
Steady-state Error (%)	0.0222	0.0444	0.1521	0.0698

Table 3: Summary of Results for EMK Controller Simulation

tem (refer to Table 1), the directional control assembly requires a larger magnitude of control effort as compared to the primary subsystem for both steering profiles. The performance of the control algorithm is further evaluated in terms of three performance measures: (i) Peak error (in %), (ii) Steady-state error (in %), and (iii) Settling time (in seconds). These are tabulated as shown in the Table 2. Here, 5% settling time is considered for Case 2 only. This performance measure will not be considered with Case 1.

For the second set of simulations, the control algorithm proposed in Section 6 was simulated on the same system as described in (1) and (2) having the same parameters as given in Table 1. However, the estimated torques are used to generate the target dynamics per (27) as opposed to “measured” torques that were available in the previous set of simulations. The driver experience and locked tracking errors, $e_1(t)$ and $e_2(t)$, are shown in Figure 6. The errors $e_1(t)$ and $e_2(t)$ are within ± 0.01 rad for both cases. The corresponding control torques, $T_1(t)$ and $T_2(t)$, are shown in Figure 7. The torque estimate values $\hat{\tau}_1$ and $\hat{\tau}_2$ are shown in Figure 8. Here it is observed that the driver input torque, $\tau_1(t)$ shown in Figure 3 is accurately observed by the signal $\hat{\tau}_1(t)$ shown in Figure 8. These numerical results indicate the feasibility of using torque observation values in the control algorithm thus eliminating the need for the introduction of torque transducers in the steering system hardware. As with the previous set of simulations, the performance is evaluated using peak error and steady-state error performance measures, and the results are tabulated in Table 3

To evaluate the steering system behavior, a standard steering mechanism has been simulated whose dynamics have the form as (5). Furthermore, the lumped

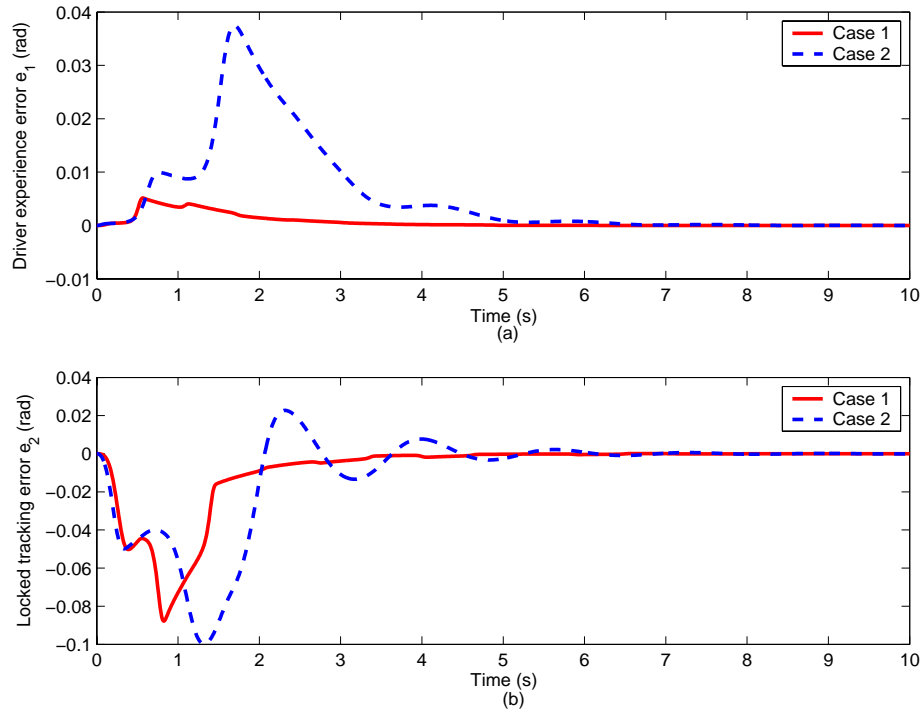


Figure 4: Adaptive Control Simulation Results: Tracking errors (a) $e_1(t)$, and (b) $e_2(t)$. The errors in both cases approach zero achieving the control objective. Selected gains can be increased for faster convergence rates at the cost of larger control effort.

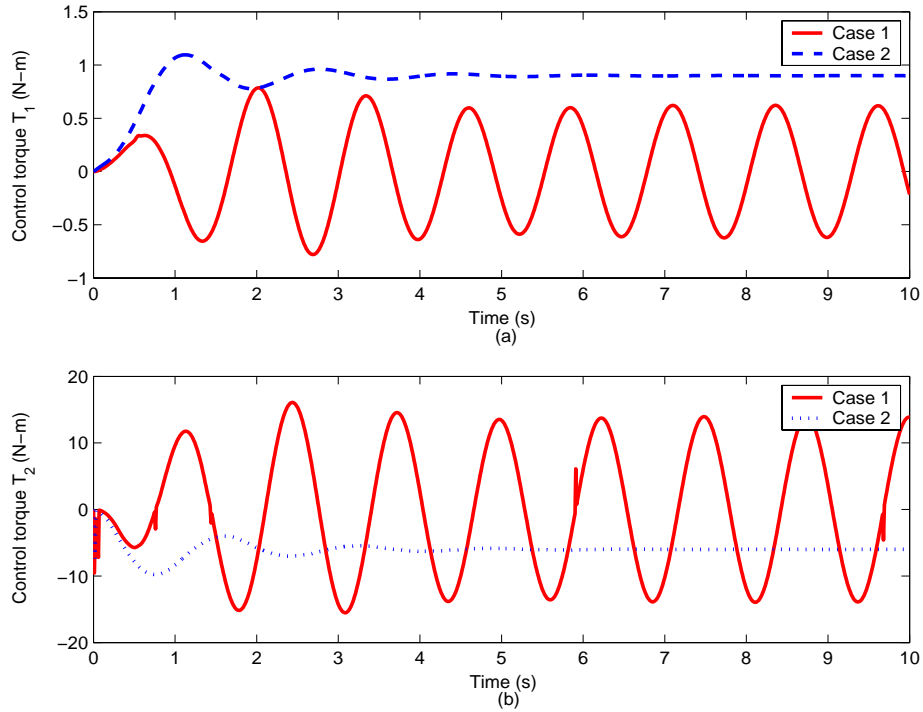


Figure 5: *Adaptive Control Simulation Results: Control torques, (a) $T_1(t)$, and (b) $T_2(t)$. To achieve the control objective, larger magnitude of control effort is required by the directional control assembly because of higher values of parameters associated with it.*

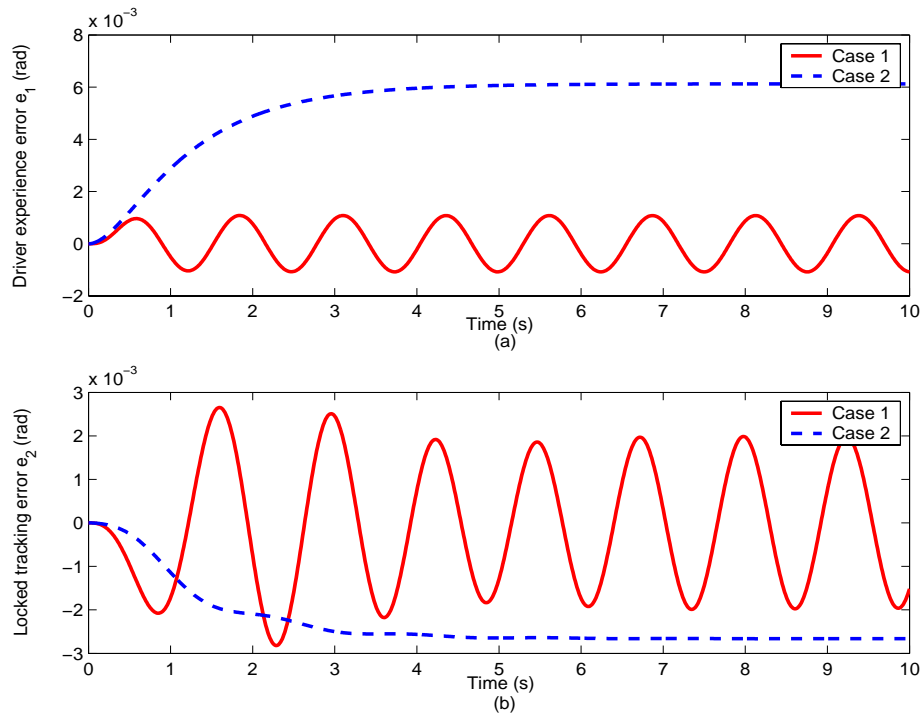


Figure 6: *EMK Controller Simulation Results: Tracking errors (a) $e_1(t)$, and (b) $e_2(t)$. Note that magnitude of errors is very small demonstrating that the control objectives were achieved.*

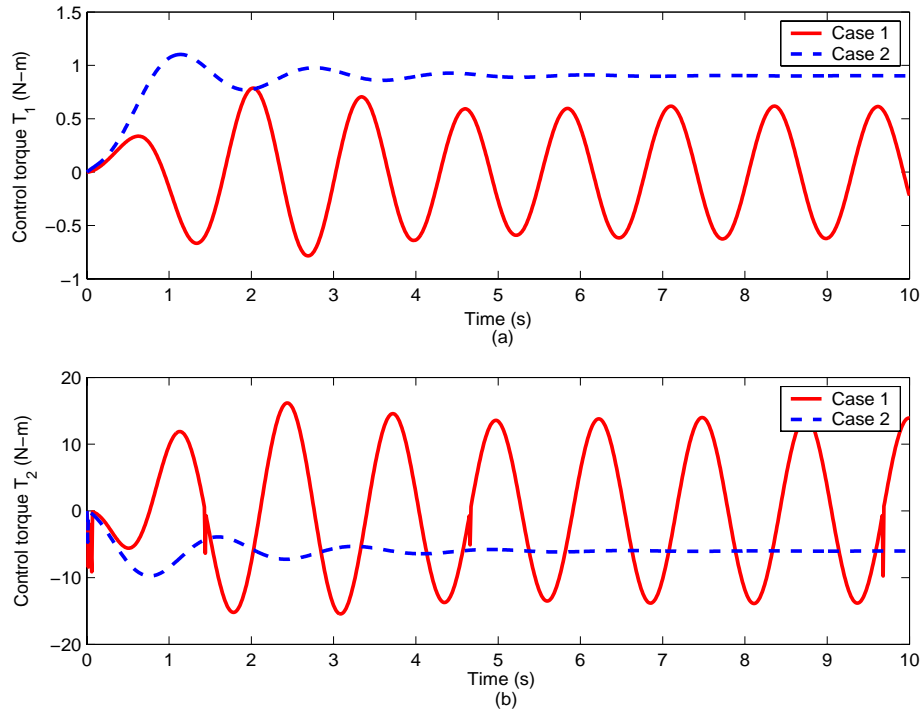


Figure 7: *EMK Controller Simulation Results: Control torques (a) $T_1(t)$, and (b) $T_2(t)$. Similar to the first set of simulations, a larger control input is required for the directional control assembly.*

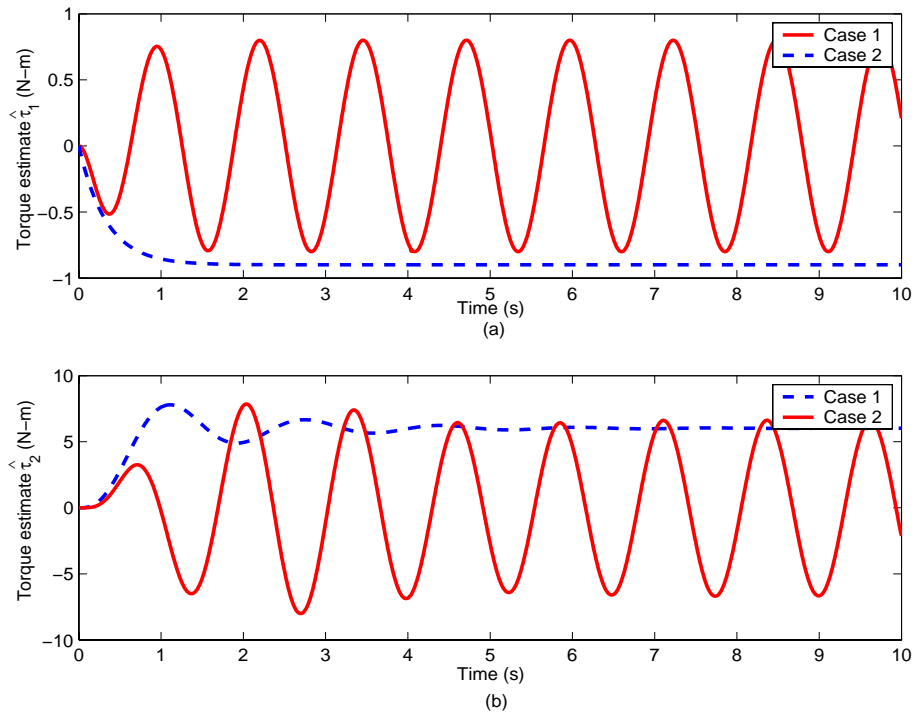


Figure 8: *EMK Controller Results: Estimated torques, (a) $\hat{\tau}_1(t)$, and (b) $\hat{\tau}_2(t)$. The torque observers in the control algorithm estimate the actual torque values eliminating the need for expensive torque sensors to be present in the system.*

model parameters are assumed to be the sum of the primary and secondary system parameters given in Table 1 so that

$$(I_1 + I_2)\ddot{\theta}_a + N_a(\theta_a, \dot{\theta}_a) = \alpha_1\tau_1 + \alpha_2\tau_2, \quad N_a(\theta_a, \dot{\theta}_a) = (B_1 + B_2)\dot{\theta}_a + (K_1 + K_2)\theta_a \quad (63)$$

To demonstrate that the driver can be provided with a tunable force feedback, the simulation was executed with a different set of target parameters. In this case, the parameter B_T was increased an order of magnitude to $0.2 \text{ kg} - \text{m}^2/\text{s}$ while all other parameters and inputs were unchanged for case 1. The results are shown in Figure (9) which shows the target system displacement, $\theta_d(t)$ for the original system and the system with increased damping along with the response of a standard steering system, $\theta_a(t)$. As can be observed, the magnitude of $\theta_d(t)$ for the system with the original parameters is greater than $\theta_a(t)$ showing that the values α_{T1} and α_{T2} can be used to provide variable power assist. Further, the magnitude of $\theta_d(t)$ for the system with the original parameters is greater than that with increased damping showing that the nature of the system response can also be varied by adjusting the target system parameters I_T , B_T , and K_T . Thus, the driver can be provided with a customized “feel” at the steering wheel by appropriately changing the target parameters for a given steer-by-wire system.

8 Experimental Results

To address some of the practical issues involved in the implementation of the control algorithm on a prototype steer-by-wire system, the proposed control laws were tested on an experimental testbench.

8.1 Experimental Setup

The experimental configuration is shown in Figure 10. It consisted of two switched-reluctance motors (SRMs) controlled using NSK drives, a steering wheel, a rack and pinion system, a hydraulic damper, and a spring. One of the SRMs provided the road feedback to the operator by means of the steering wheel, while the second motor actuated the directional control assembly. The SRMs had inbuilt resolvers that provided high resolution angular displacement measurements. Additionally, a LVDT was also used to measure the rack displacement. Optionally, the hydraulic damper and/or the spring could be connected to the rack to simulate road reaction forces. Precision torque sensors that are required for the accurate implementation of the adaptive control algorithm were prohibitively expensive to incorporate in this study, while attempts with low quality sensors were unsuccessful due to the inherent drift and noise in the sensor signals. Hence, in this experimental section, the algorithms presented in Section 6 (which do not require the measurement of torque) are implemented.

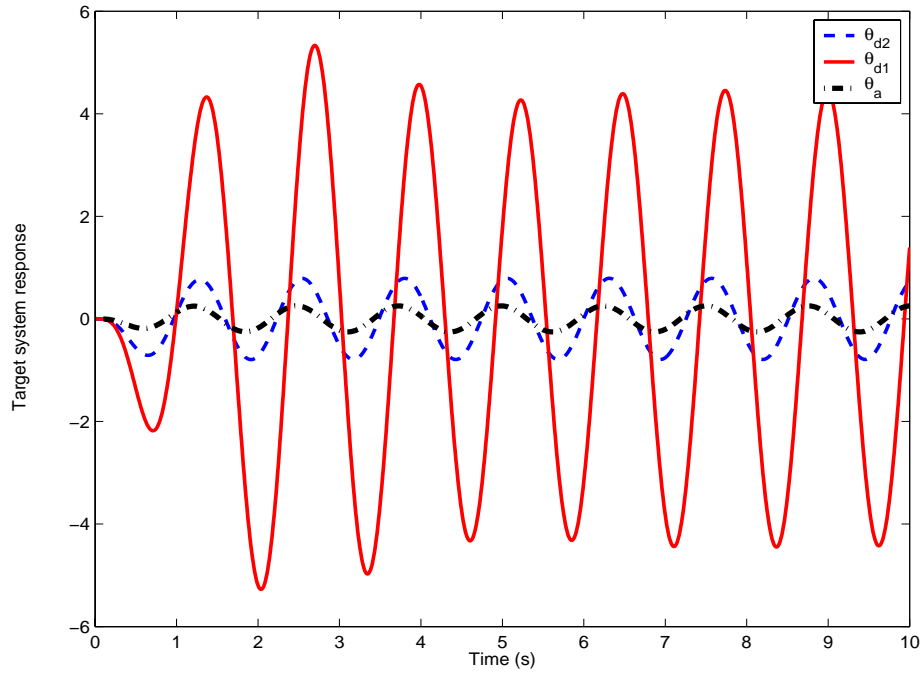
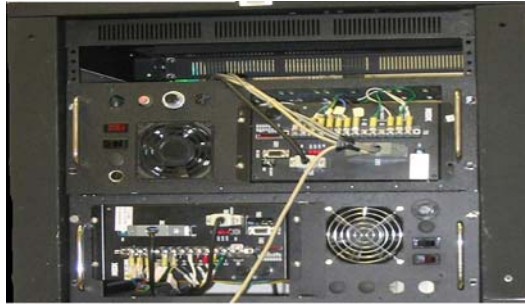
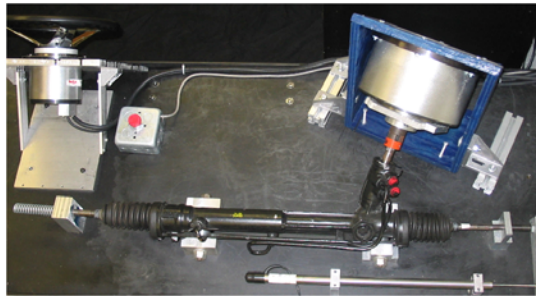


Figure 9: *EMK Controller Simulation Results: Response of system with (a) $B_T = 0.2 \text{ kg} - \text{m}^2/\text{s}$, (b) $B_T = 0.02 \text{ kg} - \text{m}^2/\text{s}$, and (c) Standard steering system response. The variable magnitudes of the responses for different values of target parameters, damping in this case, show that the feel of the steering wheel can be made lighter or heavier depending on the operator's need and comfort.*



(a)



(b)

Figure 10: *Laboratory Experimental Setup: (a) NSK Motor Drives, (b) Steering Wheel, Rack and Pinion System. This setup created a steer-by-wire steering system similar to one that can be used in a ground vehicle to experimentally validate the proposed control algorithm. Notice that the essential components are quite the same as shown in Figure 2.*

Performance Measure	Case 1		Case 2	
	e_1	e_2	e_1	e_2
Peak Error (%)	1.5	3.2	5.2	2.5
Steady-state Error (%)	1.5	2.0	5.2	2.39

Table 4: Summary of Results for Experimental Evaluation

An AMD Athlon 1.2 GHz PC running QNX 6.2 RTP (Real Time Platform), a real-time micro-kernel based operating system, provided the computational power to implement the control algorithms. An in-house graphical user interface program, Qmotor 3.0, ensured real-time execution of the control algorithms written in “C++”. This also facilitated real time graphing, data logging and on-line gain tuning. Data acquisition and control implementation were performed at a frequency of 1.0 kHz using the ServoToGo I/O board.

To study and evaluate the effect of this haptic interface feedback system, the system was also equipped with a virtual reality environment. This consisted of a 60” X 80” screen along with a high capacity projector which provided the visual feedback for driver-in-loop experiments. A MATLAB-based system was built both, to simulate the vehicle chassis dynamics as well as to render a VRML scene in real-time. Alternate input devices such as a joystick incorporating force feedback were also considered to provide assistance to handicapped drivers.

8.2 Tests and Results

Preliminary tests were performed to determine the system parameters listed in Table 1. The target dynamics were generated as shown in (27). Again, experiments were performed for the two cases as specified in the previous section. For each case, the gains were tuned until the best system performance was obtained. The values of the target system parameters, I_T , B_T , and K_T were chosen in the previous section and listed in Table 1. The experimental results for driver experience error $e_1(t)$, and locked tracking error $e_2(t)$ are shown in Figure 11. As with the simulations, the performance of the control algorithm in an experimental test is evaluated using the same performance indices as the EMK controller simulation. The results are shown in Table 4.

As can be viewed from Figure 11, the errors $e_1(t)$ and $e_2(t)$, have small magnitudes for both the maximum and steady-state values in each case. The steady-state errors for the case of the step input (case 2) is mainly due to the large static friction present in the physical system which was very hard to compensate for. As in the simulations, these error values show that $\theta_1(t)$ tracks the reference trajectory $\theta_d(t)$ and that $\theta_2(t)$ follows $\theta_1(t)$ (and hence achieves the two control objectives outlined). The actual

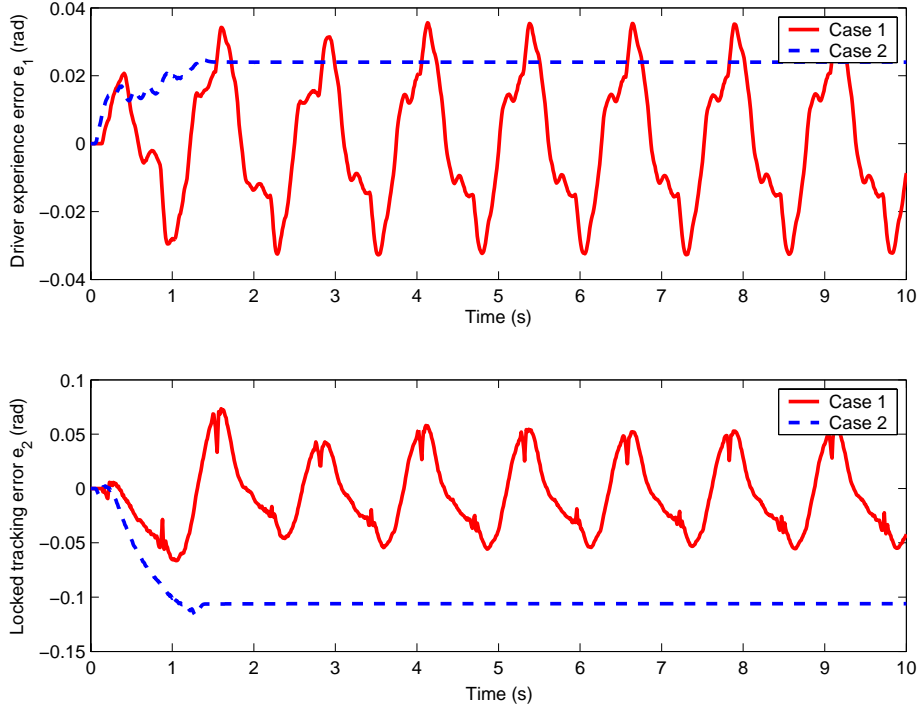


Figure 11: *Experimental Results: Tracking errors $e_1(t)$, and $e_2(t)$. As shown in the simulation results, small magnitude of the errors demonstrates the validity of proposed control algorithm.*

driver input torques, $\tau_1(t)$, for both cases, and their estimates, $\hat{\tau}_1(t)$, are shown in Figure 13. The values for the control torques $T_1(t)$ and $T_2(t)$ are shown in Figure 12.

The target system response for all the simulation and experimental tests have been plotted in Figure 14. Since $e_1(t)$ and $e_2(t)$ are small in magnitude in comparison to the target trajectories, in effect, the target system response is indeed the actual response of the system.

9 Conclusion

In this paper, the design of an adaptive, nonlinear tracking controller has been presented which ensures that: *i)* the directional control assembly follows the driver commanded input, and *ii)* the dynamics of the driver input device follows that of a target system. A complete stability analysis, using Lyapunov-based techniques, has been presented to demonstrate that the proposed control law guarantees global asymptotic regulation of the “locked tracking error” and the “driver experience tracking error”. An extension was presented that eliminated torque measurements and developed an

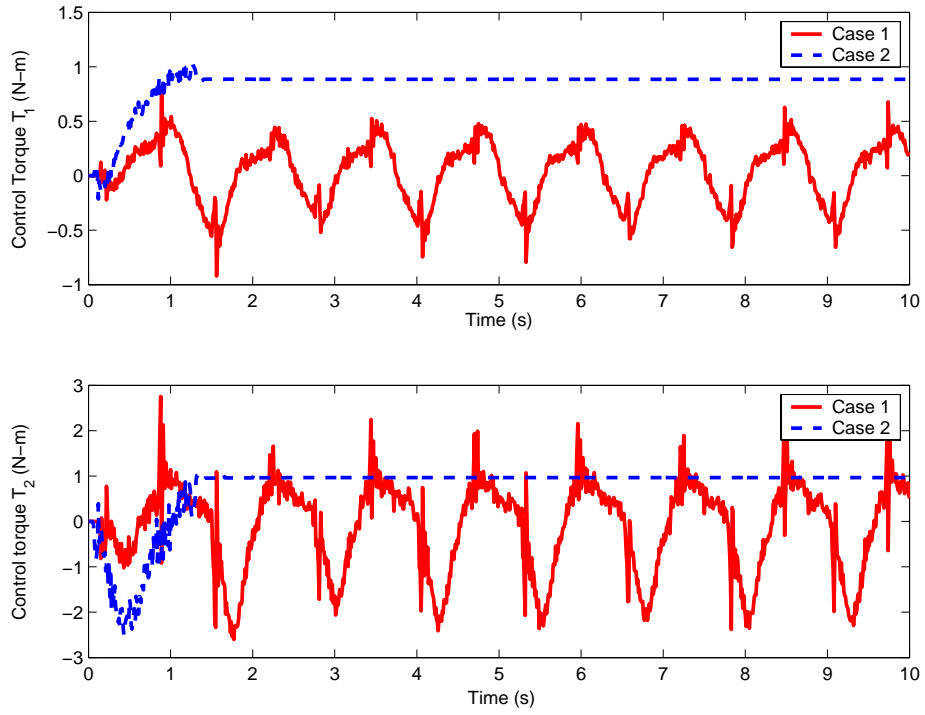


Figure 12: *Experimental Results: Control Torques $T_1(t)$, and $T_2(t)$. Experimentally as well, the control input torques follow a similar pattern as in the simulations. One of the differences though is the inherent noise in the experimental system.*

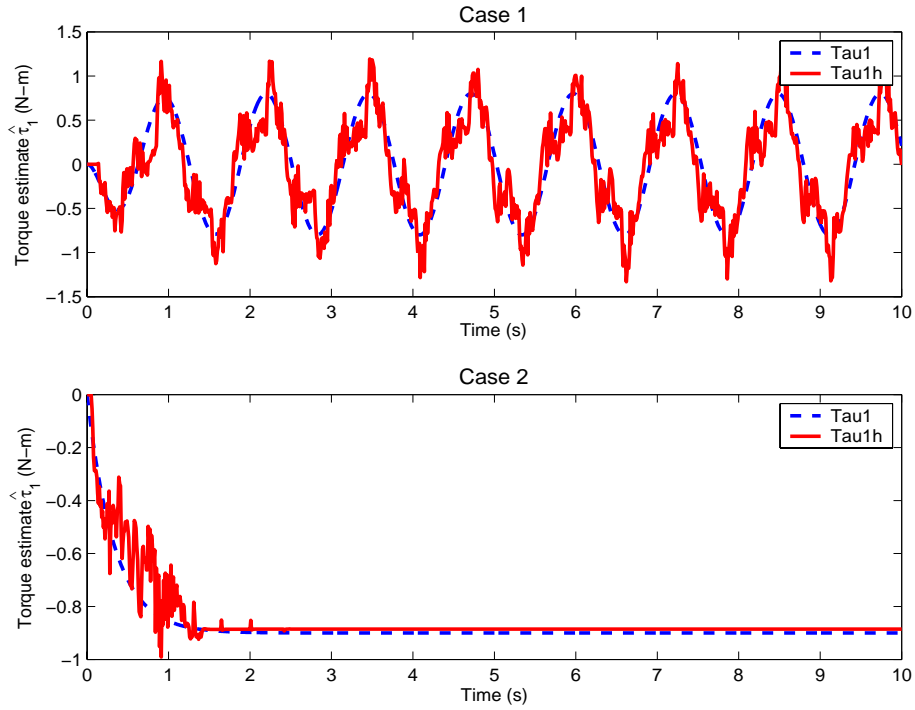


Figure 13: *Experimental Results: Actual and estimated driver input torques, $\tau_1(t)$ and $\hat{\tau}_1(t)$ for (a) Case 1, and (b) Case 2. The estimated values shown here and small magnitude of error values in Figure 11 prove the efficacy of the controller and the ability of torque observers to accurately estimate input torque values.*

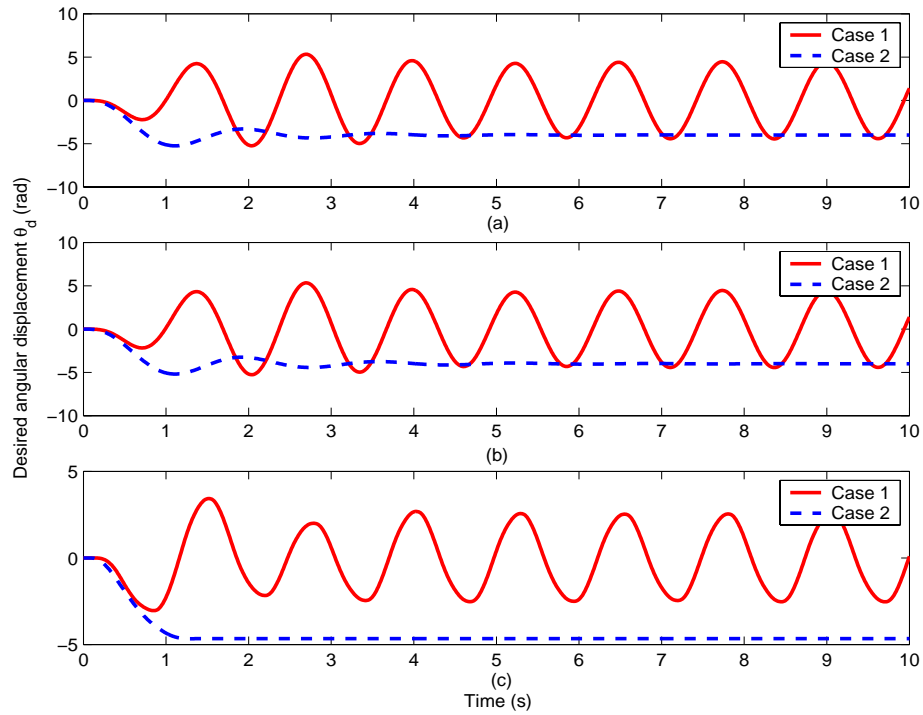


Figure 14: *Target System Responses: (a) Adaptive Controller, (b) EMK Controller, and (c) Experimental Results. During the experiment, operator could feel the steering wheel become lighter or heavier and the system response differ for different sets of target parameters.*

exact model knowledge tracking controller. Representative numerical simulation results have been presented to validate the performance of the proposed control law. A detailed description of an experimental test setup has been presented along with experimental verification of the control algorithm.

References

- [1] Dawson, D., Hu, J., and Burg, T., *Nonlinear Control of Electric Machinery*, Marcel Dekker, 1998.
- [2] Desoer, C. A., and Vidyasagar, M., “*Feedback Systems: Input-output Properties*”, Academic Press, 1975.
- [3] Gillespie, B. R., Hasser, C., and Tang, P., “Cancellation of Feedthrough Dynamics Using a Force-Reflecting Joystick” *proceedings of the ASME International Mechanical Engineering Conference and Exposition*, Nashville, TN, Vol. 67, pp. 319-329, November 1999.
- [4] Godley, S. T., Triggs, T. J., and Fildes, B. N., “Driving Simulator Validation for Speed Research”, *Accident Analysis and Prevention*, Vol. 34, Issue 5, pp. 589-600, September 2002.
- [5] Huh, K., Seo, C., Kim, J., and Hong, D., “Active Steering Control Based on the Estimated Tire Forces”, *proceedings of the American Control Conference*, San Diego, CA, pp. 729-733, June 1999.
- [6] Lee, D., and Li, P. Y., “Passive Control of Bilateral Tele-operated Manipulators: Robust Control and Experiments”, *proceedings of the American Control Conference*, Arlington, VA, pp. 4612-4618, June 2001.
- [7] Liu, A., and Chang, S., “Force Feedback in a Stationary Driving Simulator”, *proceedings of the IEEE International Conference on Systems, Man and Cybernetics*, Vol. 2, Vancouver, Canada, pp.1711-1716, 1995.
- [8] Lewis, F. L., Abdallah, C. T., and Dawson, D. M., *Control of Robot Manipulators*, Macmillan Publishing Company, 1993.
- [9] Mills, V., Wagner, J., Dawson, D., “Nonlinear Modeling and Analysis of Steering Systems for Hybrid Vehicles”, *proceedings of ASME International Mechanical Engineering Congress and Exposition*, New York, NY, pp. 571-578, November 2001.
- [10] Mills, V. and Wagner, J., “Behavioral Modeling and Analysis of Hybrid Vehicle Steering Systems”, *proceedings of Institution of Mechanical Engineers, Part D, Journal of Automobile Engineering*, Vol. 217, no. 5, pp. 349-361, 2003.

- [11] Post, J. W., and Law, E. H., “Modeling, Simulation and Testing of Automobile Power Steering Systems for the Evaluation of On-Center Handling”, *SAE Paper* No. 960178, 1996.
- [12] Qu, Z., and Xu, J., “Model Based Learning Controls and their Comparisons using Lyapunov Direct Method” *Asian Journal of Control, Special Issue on Learning Control*, Vol. 4, No.1, pp. 99-110, March 2002.
- [13] Rossetter, E. J., Switkes, J. P., and Gerdes, J. C., “A Gentle Nudge Towards Safety: Experimental Validation of the Potential Field Driver Assistance System”, *proceedings of the American Control Conference*, Denver, CO, pp. 3744-3749, June 2003.
- [14] Ryu, J., and Kim, H., “Virtual Environment for Developing Electronic Power Steering and Steer-by-Wire Systems”, *proceedings of the IEEE/RSJ International Conference on Intelligent Robots and Systems*, pp. 1374-1379, Kyongju, Korea, 1999.
- [15] Setlur, P., Dawson, D., Wagner, J., and Fang, Y., “Nonlinear tracking Controller Design for Steer-by-Wire Systems”, *proceedings of the American Control Conference*, Anchorage AK, pp. 280-285, May 2003.
- [16] Slotine, J. J. and Li, W. “*Applied Nonlinear Control*”, Prentice Hall, 1991.

A Appendix A

The explicit definitions for $Y_1(\cdot)$, $Y_2(\cdot)$, ϕ_1 , and ϕ_2 are given as follows

$$Y_1(\theta_1, \dot{\theta}_1, \tau_1, \ddot{\theta}_{d1}, \dot{\theta}_{d1}) = \begin{bmatrix} Y_{N1} & -\tau_1 & \ddot{\theta}_{d1} + \mu_1 \dot{e}_1 \end{bmatrix}$$

$$\phi_1 = \begin{bmatrix} \phi_{N1} & \alpha_1 & I_1 \end{bmatrix}^T$$

$$Y_2(\theta_1, \dot{\theta}_1, \theta_2, \dot{\theta}_2, \tau_1, \tau_2, T_1) = \begin{bmatrix} -Y_{N1} & \tau_1 & T_1 & Y_{N2} & -\tau_2 & \mu_2 \dot{e}_2 \end{bmatrix}$$

$$\phi_2 = \begin{bmatrix} \frac{I_2}{I_1} \phi_{N1} & \frac{I_2}{I_1} \alpha_1 & \frac{I_2}{I_1} & \phi_{N2} & \alpha_2 & I_2 \end{bmatrix}^T$$

where Remark 1 has been utilized.

B Appendix B

Equation (48) can be integrated and rewritten as

$$\begin{aligned}
V_{a1}(t) - V_{a1}(t_0) = & -K_s \int_{t_0}^t s_1^2(\sigma) d\sigma \\
& + \int_{t_0}^t p_1(\sigma) (-\eta_1(\sigma) - \rho_1 \operatorname{sgn}(p_1(\sigma))) d\sigma \\
& + \left[\int_{t_0}^t \frac{dp_1(\sigma)}{d\sigma} (-\eta_1(\sigma) - \rho_1 \operatorname{sgn}(p_1(\sigma))) d\sigma \right].
\end{aligned} \tag{64}$$

The bracketed term in this expression is further evaluated as follows

$$\begin{aligned}
\int_{t_0}^t \frac{dp_1(\sigma)}{d\sigma} (-\eta_1(\sigma) - \rho_1 \operatorname{sgn}(p_1(\sigma))) d\sigma = & \left[- \int_{t_0}^t \frac{dp_1(\sigma)}{d\sigma} \eta_1(\sigma) d\sigma \right] \\
& - \rho_1 \int_{t_0}^t \frac{dp_1(\sigma)}{d\sigma} \operatorname{sgn}(p_1(\sigma)) d\sigma.
\end{aligned} \tag{65}$$

After integrating the bracketed term in (65) by parts, we have

$$\begin{aligned}
\int_{t_0}^t \frac{dp_1(\sigma)}{d\sigma} (-\eta_1(\sigma) - \rho_1 \operatorname{sgn}(p_1(\sigma))) d\sigma = & - \left[\eta_1(\sigma) p_1(\sigma) \Big|_{t_0}^t - \int_{t_0}^t p_1(\sigma) \frac{d\eta_1(\sigma)}{d\sigma} d\sigma \right] \\
& - \rho_1 |p_1(\sigma)| \Big|_{t_0}^t.
\end{aligned} \tag{66}$$

After substituting (66) into (64), the following expression is obtained

$$\begin{aligned}
V_{a1}(t) - V_{a1}(t_0) = & -K_s \int_{t_0}^t s_1^2(\sigma) d\sigma \\
& + \int_{t_0}^t p_1(\sigma) \left(-\eta_1(\sigma) + \frac{d\eta_1(\sigma)}{d\sigma} - \rho_1 \operatorname{sgn}(p_1(\sigma)) \right) d\sigma \\
& - \eta_1(t) p_1(t) - \rho_1 |p_1(t)| + \eta_1(t_0) p_1(t_0) + \rho_1 |p_1(t_0)|
\end{aligned} \tag{67}$$

which can be simplified as follows

$$\begin{aligned}
V_{a1}(t) - V_{a1}(t_0) \leq & -K_s \int_{t_0}^t s_1^2(\sigma) d\sigma \\
& + \int_{t_0}^t |p_1(\sigma)| \left(|\eta_1(\sigma)| + \left| \frac{d\eta_1(\sigma)}{d\sigma} \right| - \rho_1 \right) d\sigma \\
& + |p_1(t)| (|\eta_1(t)| - \rho_1) + \eta_1(t_0) p_1(t_0) + \rho_1 |p_1(t_0)|
\end{aligned} \tag{68}$$

where the following equality has been used

$$p_1(\sigma) \operatorname{sgn}(p_1(\sigma)) = |p_1(\sigma)|. \quad (69)$$